Jinst

Published by IOP Publishing for Sissa Medialab

Received: *December 26, 2018*
Accepted: *February 8, 2019*
Published: *February 21, 2019*

Conceptual design of a large pixelated CZT detector with four-hole collimator matched pixel detector for SPECT imaging: a Monte Carlo simulation study

N. Boutaghane,[a,b] **B. Bouzid**[a] **and H. Zaidi**[c,d,e,f,1]

[a] *SNIRM Laboratory, Faculty of Physics, University of Science and Technology Houari Boumediene (USTHB), BP 32 El-Alia, Algiers, Algeria*

[b] *Department of Physics, Fréres Mentouri University, Constantine, Algeria*

[c] *Division of Nuclear Medicine and Molecular Imaging, Geneva University Hospital, CH-1211 Geneva, Switzerland*

[d] *Geneva University Neurocenter, CH-1205 Geneva, Switzerland*

[e] *Department of Nuclear Medicine and Molecular Imaging, University of Groningen, University Medical Center Groningen, 9700 RB Groningen, Netherlands*

[f] *Department of Nuclear Medicine, University of Southern Denmark, DK-500, Odense, Denmark*

E-mail: habib.zaidi@hcuge.ch

Abstract: Significant progress has been achieved in the design of pixelated CZT detectors dedicated to cardiac and breast SPECT imaging. However, their detector geometry and associated collimators' design have limited their clinical use. The aim of this work is to determine the best combination between a large pixelated CZT detector and parallel-hole collimator that can provide high spatial resolution at low injected activity with low-energy radiotracers. Our proposed combination resulted in the design of a novel four-hole matched pixel detector (4-HMPD) configuration. Our novel 4-HMPD design based on large pixelated CZT detector was firstly compared to the standard one-hole matched pixel detector (1-HMPD) configuration using Monte Carlo simulation. We have also predicted the influence of pixel size, interpixel gap and source-to-collimator distance on the basis of resulting spatial resolution, sensitivity and crosstalk events fraction for three collimator hole lengths for Tc-99m (140 keV). Thereafter, we used the same detector and collimator settings of the 1-HMPD configuration as constructed with the D-SPECT camera module (Redlen Technologies, BC, Canada) for our 4-HMPD design to compare the performance of the two configurations. Our preliminary results showed that a large pixel size, a small interpixel gap and a small collimator hole

[1] Corresponding author.

https://doi.org/10.1088/1748-0221/14/02/P02026

2019 JINST 14 P02026

length increased significantly the sensitivity at the detriment of spatial resolution. The performance comparison between the 4-HMPD and the 1-HMPD configurations demonstrated an improved reconstructed spatial resolution (by a factor two), higher contrast with the large sphere of the modified Jaszczak phantom (from 63.1% to 39.1%), clear appearance of cold spheres (> 14 mm diameter) and the cold cylinders (> 11.1 mm diameter). The crosstalk events fraction varied from 8.5% to 12.8%. Our novel detector/collimator combination allows less electronic readout complexity, less crosstalk events between pixels and twofold increase in septal thickness resulting in low septal penetration compared to the classical 1-HMPD configuration. It also showed the highest enhancement in terms of spatial resolution even in cases of low sensitivity with less injected activity, and outperformed the performance of existing conventional NaI (TI) crystal-based systems.

KEYWORDS: SPECT, CZT detector, parallel-hole collimator, Monte Carlo, crosstalk

2019 JINST 14 P02026

Contents

2019 JINST 14 P02026

1 Introduction

Conventional large field-of-view NaI(TI) crystal-based single-photon emission computed tomography (SPECT) cameras are widely used in clinical nuclear imaging [1]. However, their shortcomings namely the indirect signal conversion and low energy resolution have stimulated the introduction of new generation solid-state-based detectors [2–5]. Cadmium Zinc Telluride (CZT)-based cameras are currently used in clinical routine, especially in cardiac and breast imaging applications [6–10]. A number of studies confirmed the clinical benefits of the improved performance of these dedicated systems [11], as technologies enabling to reduce the acquisition time [12, 13] and/or decrease the injected activity to patients [14]. However, it remains a matter of controversy within the nuclear medicine community whether the improved performance of these new dedicated detectors is due only to the CZT material and its pixelated configuration or the geometry of the collimator with the Tungsten material or a combination of both. In addition, these dedicated systems use multiple fixed or movable small detector modules to increase sensitivity [15]. Moreover, their detector geometry and associated collimator configuration have limited their use for imaging few organs or organ systems [16, 17]. In addition, the high cost and limited availability of dedicated CZT systems hampered their widespread use in the clinic, thus impacting the gathering of large databases for multicenter validation studies. As a consequence, further research and development efforts are required to optimize the design of these systems to challenge the popularity of conventional SPECT cameras. To this end, three general purpose SPECT systems have been recently developed, namely the Discovery NM/CT 670 CZT (General Electric Healthcare) [18], the Veriton system (Spectrum Dynamics) and the Valiance X12 prototype (Molecular Dynamics) [19]. In fact, these cameras are

equipped with a fixed parallel-hole collimator used with most gamma-emitting radionuclides. In particular, a preliminary study was performed with medium energy ^{177}Lu-octreotate tracer [20].

In each specific imaging examination with gamma-emitting radionuclides, the energy and other important information related to the clinical indication, e.g. high sensitivity required for cardiac imaging [21] or high spatial resolution required for brain imaging [22], dictate the selection of the collimator. However, the change of collimators is not permitted for large pixelated CZT detectors owing to the high risk of detector damage and problems associated with matching the collimator hole with the detector pixel. Hence, the collimation becomes a performance limiting component for large pixelated CZT SPECT imaging detectors. For applications requiring high sensitivity, an approach involving a large pixel detector matched collimator hole of a large pixelated CZT detector was proposed by Weng et al. [23]. Another approach involving the use of large collimator hole matched with four pixels detector was also proposed by Suzuki et al. [24]. Indeed, the wide pixel detector and hole collimator increase the sensitivity but cannot provide high spatial resolution. Another concept of mountable parallel-hole collimators were proposed by Lee and Kim [25] for preclinical imaging to overcome the trade-off between the sensitivity and spatial resolution. In the HiSens architecture, Robert et al. [26] proposed an electronically based 3D positioning algorithm that enables the use of the depth of interaction (DOI) information and several virtual sub-pixels per collimator hole without increasing the number of readout channels. They also confirmed that these virtual sub-pixels were the feature improving the achievable trade-off between spatial resolution and sensitivity.

For high spatial resolution applications, the use of a divergent collimator and small pixel CdTe semiconductor detector for an ultra-high resolution camera was proposed by Ogawa and Muraishi [27]. Another study reported on the use of parallel-slit collimator and small pixels of spinning strip CZT SPECT detector [28]. However, the drawback of using small pixels is the additional complexity, the cost of electronic reading and the increase of crosstalk events leading to charge sharing between pixels [29, 30]. Another alternative consists in using an existing dedicated cardiac D-SPECT camera [31] without any geometrical modifications to investigate potential applications in brain imaging [32]. The authors reported less than optimal performance in terms of striatal activity estimation and recommended to use a novel design of the D-SPECT system to improve the performance for brain imaging. However, the special geometrical design of this camera and its unique scanning pattern has limited its applications for whole-body SPECT imaging.

Given the above described constraints, the optimal combination between collimator and detector characteristics is sought. In this simulation study using GATE (GEANT4 Application for Tomographic Emission) software package [33], we focus on the assessment of the performance characteristics of a novel combination of large pixelated detector modelled in conjunction with the 4-HMPD configuration to the same detector modelled in conjunction with the 1-HMPD configuration. The novel proposed combination can provide high spatial resolution at low injected activity for low energy radiotracers (140 keV).

2 Materials and methods

2.1 Monte Carlo simulations

Monte Carlo simulations are commonly used to aid in the design of new detector configurations and to optimize performance parameters. Simulations were performed to assess the resulting image

2019 JINST 14 P02026

Table 1. Collimator specifications.

Collimator type	Hole length (mm)	Hole width (mm)	Septal thickness (mm)
1-HMPD	21.7	2.26	0.2
4-HMPD	21.7	1.03	0.2

quality of our proposed 4-HMPD design using GATE toolkit. The physical processes of photons interaction with matter were modelled using the GEANT4 package. The spatial and energetic blurring using Gaussian distributions were considered for every event prior to data binning.

Various pixelated CZT detector configurations with different detector and collimator characteristics combination were adopted on commercial SPECT imaging devices. Our novel 4-HMPD design was compared to the standard one-hole matched pixel detector (1-HMPD) configuration. We also assessed the influence of different pixel size (2, 2.16, 2.26 and 2.36 mm), interpixel gap (100, 200, 300 and 460 μm) and source-to-collimator distance (2, 5, 10, 15 and 20 cm) on the basis of resulting spatial resolution, sensitivity and crosstalk events fraction for three collimator hole lengths (15.7, 21.7 and 27.7 mm) at the commonly used energy (140 keV) in SPECT imaging. For the sake of performance comparison, the two previous large pixelated SPECT camera configurations were simulated. One corresponds exactly to the D-SPECT camera module (Redlen Technologies, BC, Canada) while the second keeps the same pixel dimensions, but with each collimator hole subdivided into four holes of equal size.

2.2 Geometry modelling

A large field-of-view CZT detector with 64×64 pixels array, 2.46 mm pitch size, 0.2 mm interpixel gap and 5 mm crystal thickness surrounded with lead shielding was modelled using the GATE simulation toolkit. Each pixel detector is registered with a parallel-hole collimator for the hole matched pixel detector (1-HMPD) and each pixel detector is registered to 2×2 holes array with the four-hole matched pixel detector (4-HMPD) configuration. The two configurations used are illustrated in figure 1 and the corresponding collimators specifications presented in table 1. The output data were acquired and analysed using ROOT CERN framework. All the simulations were run on a parallel computing cluster consisting of 112 cores installed in our laboratory.

2.3 Capillary line source

A line source (1 mm diameter and 10 cm length) filled with an activity of 37 MBq of ^{99m}Tc was modelled to evaluate the sensitivity and spatial resolution. An acquisition time of 120 sec and 10% photopeak energy window wide [133–147 keV] centred at 140 keV were considered owing to the high energy resolution of the CZT detector. The same acquisition parameters with a large energy window [0–170 keV] were also used to derive the energy spectra.

2.4 Modified triple line source NEMA phantom

To evaluate quantitatively the reconstructed spatial resolution, the modified triple line source NEMA phantom containing 3 linear sources of 1 mm diameter each was simulated. One was positioned at the centre of the phantom while the other two were placed at 5.5 cm distances along X and Y

2019 JINST 14 P02026

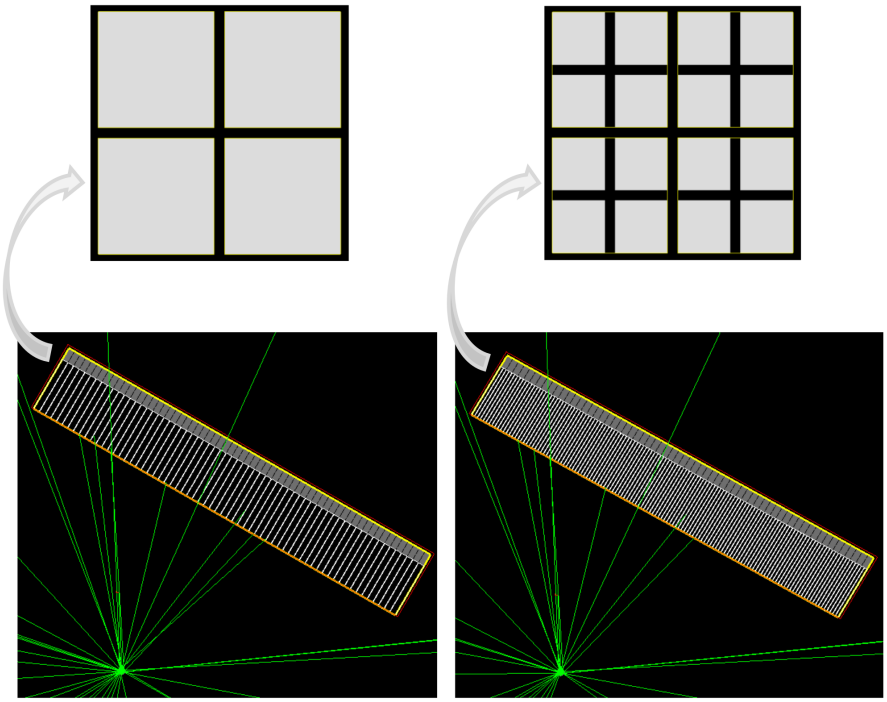

Figure 1. Schematic design of the large pixelated CZT detector with 1-HMPD configuration (left) and the 4-HMPD configuration (right). With the 1-HMPD configuration, each pixel detector is matched with each hole collimator. With the 4-HMPD configuration, each pixel detector is matched with an array of 2×2 collimator holes.

axes. An activity 18.5 MBq of ^{99m}Tc was injected in each capillary. A tomographic acquisition with 64 projections, 30 sec per view, 15 cm rotation radius and an energy pulse height window of [133 to 147 keV] were used. Image reconstruction was performed using the STIR software [34] adapted for SPECT imaging using FBP and OSEM algorithms [35], including resolution recovery (point-spread function modelling) [36, 37].

2.5 Modified Jaszczak phantom

The modified Jaszczak phantom consists of a cylinder (15.6 cm diameter and 16 cm length) containing inserts with 6 cold spheres (diameters of 12.7, 14, 18, 24, 28, and 32 mm) and 6 sectors of cold cylinders (diameters of 6.4, 7.9, 9.5, 11.1, 12.7, and 15.1 mm). This phantom was filled with 185 MBq activity of ^{99m}Tc to assess qualitatively the tomographic uniformity, reconstructed spatial resolution and contrast. The same acquisition parameters adopted for the modified triple line source NEMA phantom were used except that a 25 cm rotation radius was used instead. The tomographic data were also reconstructed (FBP algorithm) using STIR software.

2.6 Data analysis

The spatial resolution was measured by means of the full-width at half-maximum (FWHM) on the activity profile passing through the line source. Central, radial and tangential spatial resolutions were calculated on reconstructed slices of the modified triple line source NEMA phantom. The

2019 JINST 14 P02026

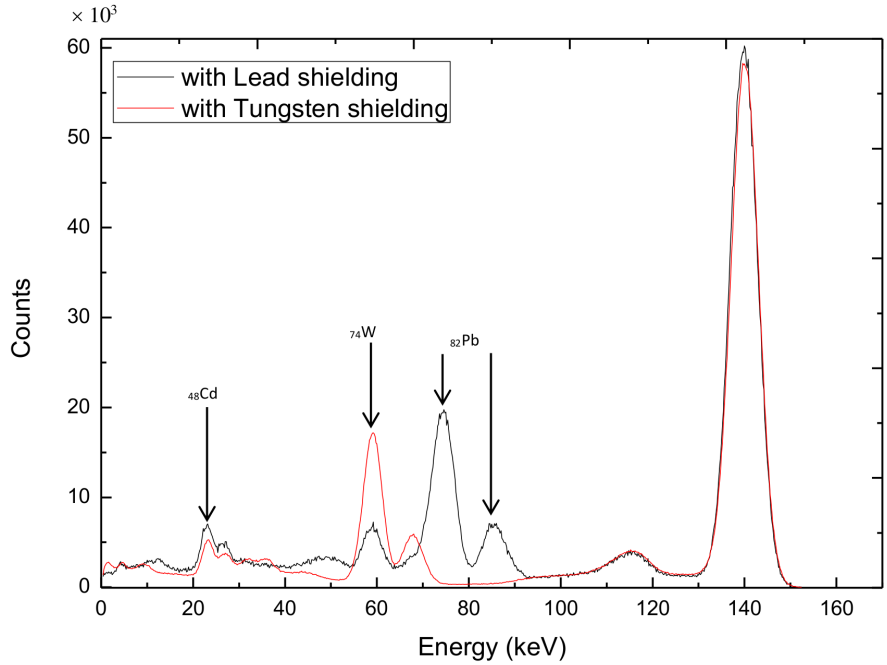

Figure 2. Simulated energy spectra obtained using a large pixelated CZT detector (1-HMPD) configuration with Tungsten and Lead shielding and ^{99m}Tc as radionuclide. The energy resolution at the photopeak (140 keV) is 6.2%.

modified Jaszczak phantom was also evaluated using three tomographic image quality metrics; namely the uniformity, spatial resolution and image contrast. The tomographic spatial resolution was qualitatively assessed by reporting the minimum diameter of cylinder seen throughout a sector of 12 successive slices. The tomographic uniformity was evaluated throughout the uniform region consisting of 8 successive slices to reveal any artefacts. Image contrast was evaluated by summing 4 successive slices containing the spheres.

3 Results

Figure 2 presents the comparison of simulated energy spectra of a line source filled with ^{99m}Tc for large pixelated CZT detector with Tungsten or Lead shielding. The characteristic x-ray peaks of Cadmium-48 ($_{48}$Cd), Tungsten-74 ($_{74}$W) and Lead-82 ($_{82}$Pb) materials were identified. A good energy resolution of about 6.2% around the central peak (140 keV) was measured. This can be regarded as a major advantage in simultaneous dual-tracer imaging [38]. As shown in figure 3, the pixelated CZT detector performance is widely determined by the position of the incident gamma interaction. The interpixel gap is totally covered by septal thickness, however, there is a fraction of crosstalk events occurring in this region. This means that all of the energy of the incident photon is absorbed by the detector but within different pixels. Hence, the incident photon is counted more than once and more than one anode would output the signal, each of them being smaller than the whole signal.

Figures 4 and 5 compare the two configurations in terms of spatial resolution and sensitivity variations with source-to-collimator distance and pixel detector size for three collimator hole lengths.

2019 JINST 14 P02026

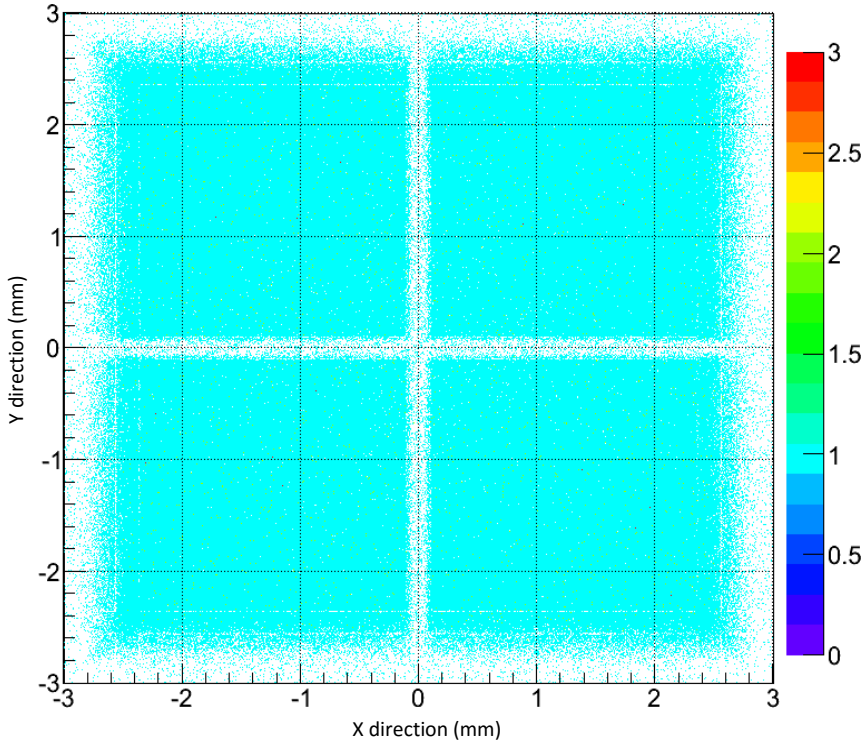

Figure 3. Crosstalk events at the interpixel gap region of a large pixelated CZT detector (only 4 pixels shown). The interpixel gap is totally covered by the septal thickness, however, there is a fraction of crosstalk events occurring in this region due to septal penetration and scatter events.

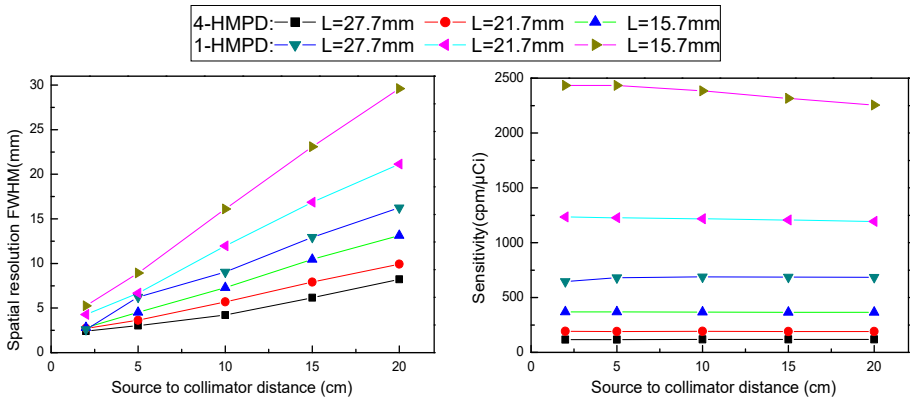

Figure 4. Plots of spatial resolution (left) and sensitivity (right) versus source detector distance for three hole lengths (27.7 mm, 21.7 mm and 15.7 mm) of the 1-HMPD and 4-HMPD configurations: the source-to-collimator distance and collimator hole length degrade significantly the spatial resolution at the detriment of sensitivity.

2019 JINST 14 P02026

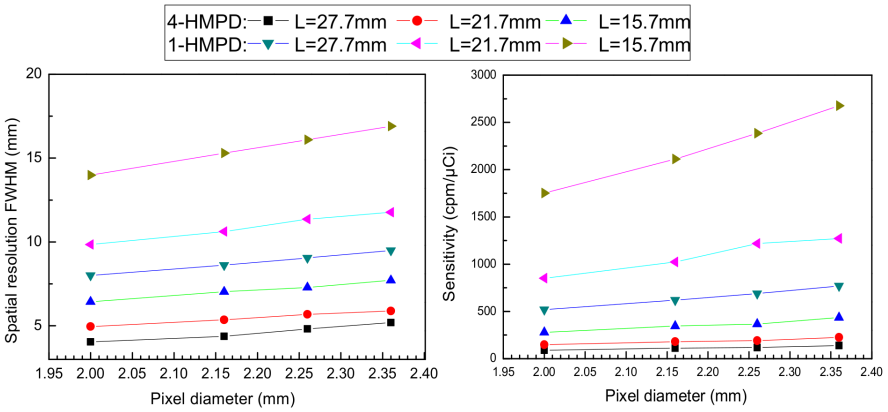

Figure 5. Plots of spatial resolution (left) and sensitivity (right) versus pixel diameter for three hole lengths (27.7 mm, 21.7 mm and 15.7 mm) of the 1-HMPD and 4-HMPD configurations. The pixel diameter increases significantly the sensitivity at the detriment of spatial resolution.

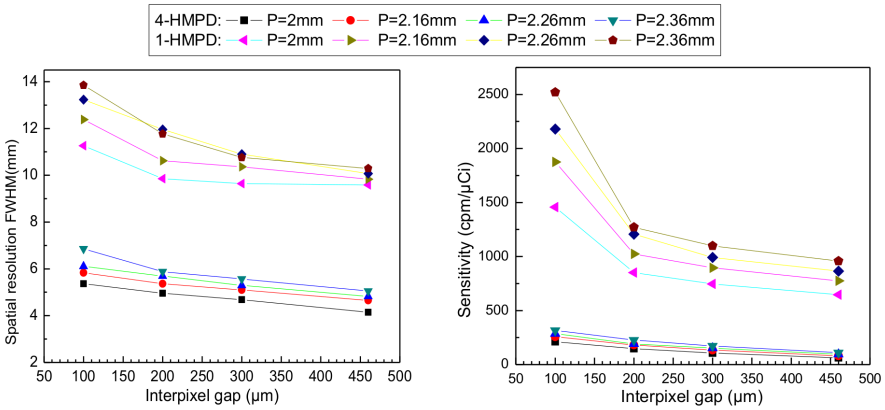

Figure 6. Plots of spatial resolution (left) and sensitivity (right) versus interpixel gap and pixel detector of the 1-HMPD and 4-HMPD configurations at fixed 21.7mm collimator hole length. The results showed that a large pixel size, a small interpixel gap increased significantly the sensitivity at the detriment of spatial resolution.

Figure 6 presents the spatial resolution and sensitivity variations with respect to septal thickness. The sensitivity decreases rapidly with septal thickness for the 1-HMPD configuration whereas this decrease is much lower for the 4-HMPD configuration.

Figure 7 compares the two configurations in terms of reconstructed spatial resolution of the modified triple line source NEMA phantom using FBP and OSEM reconstruction algorithms including PSF modeling. According to the results obtained in table 2, a very good spatial resolution was achieved in the three directions (radial, tangential and central) with the 4-HMPD configuration and FBP reconstruction, or even best with OSEM reconstruction including PSF modeling. The central reconstructed spatial resolution using OSEM algorithm including PSF modeling for both the 4-HMPD and the 1-HMPD configurations were 6.63 mm and 13.3 mm, respectively. Figure 8 compares a representative slice of the Jaszczak phantom reconstructed using FBP for the two configurations. The sphere having a diameter of 14 mm and the third sector with 11.1 mm diameter

2019 JINST 14 P02026

Table 2. Comparison of the reconstructed spatial resolution at 140 keV for 1-HMPD and 4-HMPD configurations with FBP and OSEM reconstruction algorithms including resolution recovery (PSF correction). The reconstructed spatial resolution of our 4-HMPD configuration has improved by a factor of two compared to the standard 1-HMPD configuration.

	1-HMPD		4-HMPD	
	FBP	OSEM-PSF	FBP	OSEM-PSF
Central (mm)	17.0	13.3	8.3	6.6
Radial (mm)	16.4	12.5	8.4	5.5
Tangential (mm)	11.8	9.9	6.5	5.0

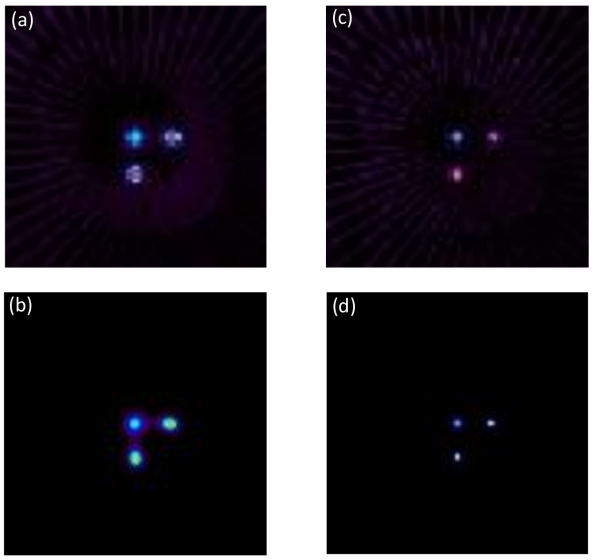

Figure 7. Reconstructed slices of the triple line source NEMA phantom simulated for the 1-HMPD configuration: (a) FBP, (b) OSEM+PSF and for the 4-HMPD configuration: (c) FBP and (d) OSEM+PSF. The higher spatial resolution achieved by the proposed 4-HMPD configuration with FBP algorithm, even best with OSEM algorithm including resolution recovery is obvious.

Table 3. Contrast values (%) of different sphere diameters of the modified Jaszczak phantom for the 1-HMPD and the 4-HMPD configurations. The 4-HMPD configuration showed the highest contrast compared to the 1-HMPD configuration.

Sphere diameter (mm)	32	28	24	18	14	12.7
1-HMPD	39.1	29.7	17.8	2.8	—	—
4-HMPD	63.1	53.8	34.2	31.2	25.1	3.1

are clearly visible for the proposed 4-HMPD configuration. The reconstructed Jaszczak phantom images for our proposed configuration provide higher contrast resolution at less injected activity. The contrast of the largest sphere was 63% and 39.1% for the 4-HMPD and 1-HMPD configurations, respectively (table 3).

2019 JINST 14 P02026

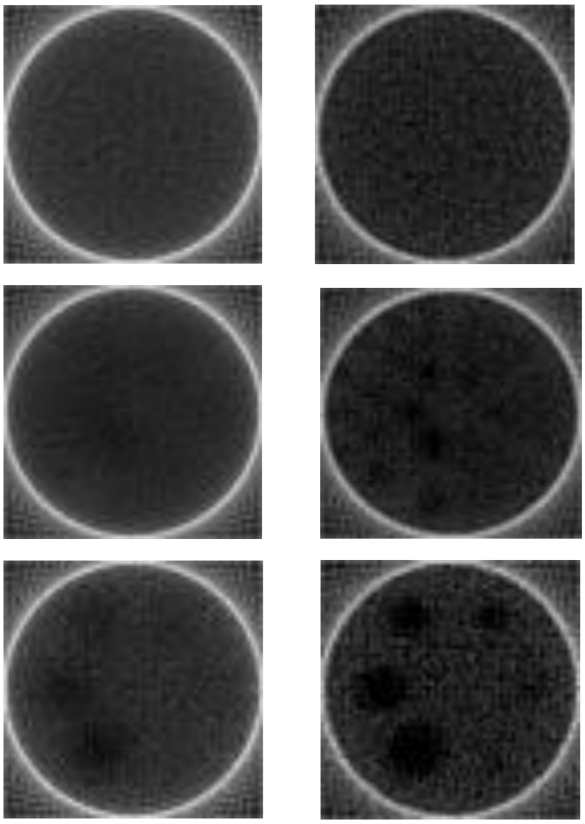

Figure 8. Representative slices of the modified Jaszczak phantom for the 1-HMPD configuration (left) and the 4-HMPD configuration (right).The 4-HMPD configuration showed the highest enhancement in spatial resolution and image contrast even under low sensitivity and less injected activity.

4 Discussion

In this simulation study, a novel configuration of matching 4-HMPD configuration for large pixelated CZT detectors is evaluated and compared to the conventional 1-HMPD configuration. The CZT detector has the ability of distinguishing fluorescent x-rays from collimator and shielding materials (figure 2). However, since they are well separated from the photopeak, fluorescent x-rays do not impact the performance of this detector. As expected from our simulations, we didn't notice an obvious tailing effect of the CZT spectrum at the lower side of the photopeak energy. This is mainly related to the detector characteristics, such as crystal thickness, hole mobility and incident gamma interaction positions. Huruska et al. [39] observed, measured and corrected this effect by combining a Monte Carlo-based method with an experimental setup for the pixelated CZT LumaGem 3200 S camera. Fritz and Shikhaliev [40] also recommended to reduce this effect in a planar CZT detector geometry by the use of tilted angle irradiation instead of normal incidence. It can be seen in figure 3 that crosstalk events of photon interaction in this region are essentially due to the contribution of septal penetration and scattered photons. The photon escapes from the prime pixel after Compton interaction and interacts with adjacent pixels and interpixel gap. As consequence, these mispositioned photons increase the charge sharing effect and deteriorate the spatial resolution.

2019 JINST 14 P02026

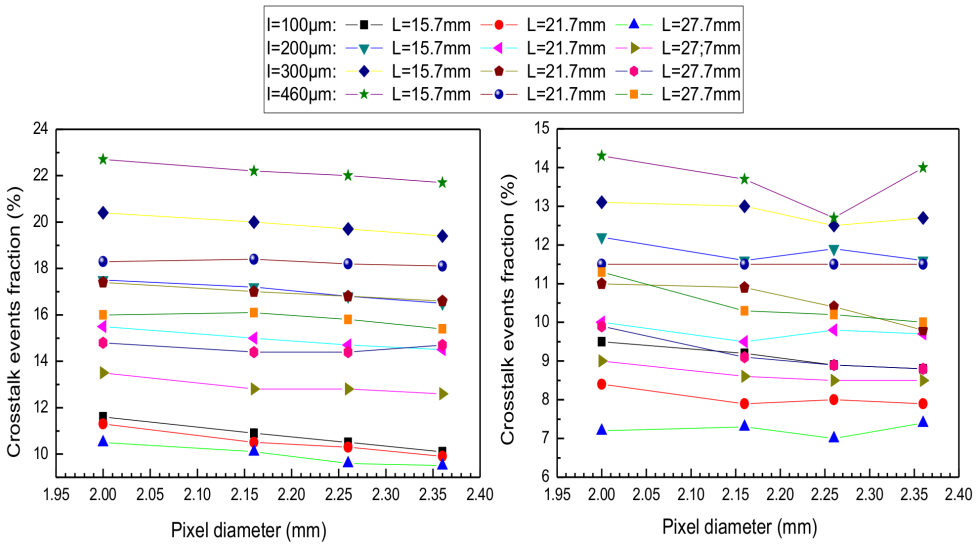

Figure 9. Plots of crosstalk events fraction versus pixel detector and interpixel gap for the 1-HMPD configuration (left) and the 4-HMPD configuration (right) for three hole lengths.

The latter will be improved if correction of the charge sharing is applied as reported by Zheng et al. [41]. Their results proposed two correction approaches based on the analysis of transient and charge sharing signals of pixelated CZT detectors. Another important issue to point out is that the intrinsic spatial resolution is equal to the pixel size, if there is no charge sharing between pixels. To this end, a quantitative analysis of pixel size and interpixel gap variation was performed to investigate the crosstalk events, responsible for the fraction of charge sharing between pixels as shown in figure 9.

The study presented by Iniewski et al. [42] also confirmed that large interpixel gap increase mostly charge sharing if the events hit the gap directly. In our case, the interpixel gap is covered by the collimator septa, however, the crosstalk events also increase with the interpixel gap. In fact, we noticed that with small interpixel gap, the crosstalk events between pixels are amplified. By increasing the interpixel gap, so many events stop at this gap, thus increasing the loss of events in this region. Bolotnikov et al. [43] also recommended that interpixel gap shouldn't be larger than 300 µm to avoid any charge loss between pixels.

As illustrated in figure 4, the smallest line slope gives always better spatial resolution variation with source-to-collimator distance. The use of large hole collimator size strongly deteriorates the spatial resolution. The solid angle of parallel-hole collimators in the CZT system is 8 times greater than conventional parallel collimators [15]. Due to the large hole acceptance solid angle, the sensitivity is improved at the cost of degradation of the spatial resolution, which implies the incorporation of resolution recovery during SPECT image reconstruction [44]. However, the reconstruction computation time with the large hole collimator takes longer compared to high-resolution collimator. Lau et al. [45] recommended that if any resolution recovery algorithm is incorporated with maximum likelihood reconstruction in cardiac examinations, a general purpose collimator should be the collimator of choice; instead of the commonly used high resolution collimator. Figure 5 also shows that the spatial resolution improves by minimizing pixel size.

2019 JINST 14 P02026

Table 4. Comparison of the spatial resolution and sensitivity between different conventional SPECT imaging systems and the proposed design for ^{99m}Tc at 10 cm source-to-collimator distance for our proposed 4-HMPD configuration.

	4-HMPD	Weng et al. [46]	Philips BrightViewXCT [49]	GE Infinia [50]
Spatial Resolution (mm)	5.7	6.9	7.4	7.4
Sensitivity (counts/min/μCi)	192	261	168	160

However, with small pixel size, there is sharing of events between adjacent pixels and the pixel where the interaction occurred. The hole width reduction used with the 4-HMPD configuration improves the spatial resolution (table 2 and figure 7) and the contrast (table 3 and figure 8) at the expense of the sensitivity. It is also obvious that the sensitivity improves by decreasing the hole collimator length or by increasing the collimator hole width. However, septal penetration increases the sensitivity but reduces image quality. To obtain a good spatial resolution with high-energy gamma emitters and to maintain an acceptable level of photon penetration within septal separation, the thick septal thickness or the higher collimator hole length must be used as shown in figure 6. However, the increase of the septal thickness is limited by the detector interpixel gap and an increase of collimator hole length is necessary with any pixelated CZT detector. An optimal septal thickness of 0.32 mm was reported in the study by Weng et al. [46] for energy independence with a large CZT detector. However, in the case of registration with the interpixel gap, it may favour events loss between pixels, which was also reported by Bolotnikov et al. [43].

Table 4 compares the performance of the 4-HMPD configuration versus various commercially available LEHR collimators and the optimized collimator with large CZT SPECT camera reported by Weng et al. [46]. The proposed 4-HMPD configuration shows promising imaging performance and outperforms the all existing conventional NaI(TI) crystal-based cameras.

Despite the promising results, our work bears a number of limitations. Firstly, there is a little fraction of detector area covered by the collimators septa resulting in sensitivity degradation. However, the physical division of the pixel detector by the four hole collimator to four quadrants might result in sub-spatial resolution under the pixel size [47]. Secondly, to evaluate effectively the performance of the CZT detector, two considerations must be taken into account: the gamma interaction model through the Monte Carlo method and the charge induced and collection model with a finite element method (COMSOL Multi Physics) [48]. The electric field and weighting potential distributions inside a detector must be calculated for better quantification of the charge induction and collection.

5 Conclusion

The performance of a large pixelated CZT detector mounted on a 4-HMPD configuration was investigated using Monte Carlo simulations. This combination allowed high spatial resolution, less electronic readout complexity, less crosstalk events between pixels and a twofold increase in septal thickness resulting in low septal penetration in the collimator. It also yielded higher image quality at reduced injected activity with an acceptable sensitivity compared to the 1-HMPD configuration and conventional SPECT cameras.

2019 JINST 14 P02026

References

[1] T.E. Peterson and L.R. Furenlid, *SPECT detectors: the anger camera and beyond*, *Phys. Med. Biol.* **56** (2011) R145.

[2] D.G. Darambara and A. Todd-Pokropek, *Solid state detectors in nuclear medicine*, *Q. J. Nucl. Med.* **46** (2002) 3.

[3] H. Zaidi, *Recent developments and future trends in nuclear medicine instrumentation*, *Z. Med. Phys,* **16** (2006) 5.

[4] E. Gordon DePuey, *Advances in SPECT camera software and hardware: currently available and new on the horizon*, *J. Nucl. Cardiol.* **16** (2012) 551.

[5] T. Sharir, P.J. Slomka and D.S. Berman, *Solid-State SPECT technology: fast and furious*, *J. Nucl. Cardiol.* **17** (2010) 7.

[6] P. Slomka, G.U. Hung, G. Germano and D.S. Berman, *Novel SPECT technologies and approaches in cardiac imaging*, *Cardiovasc. Innov. Appl.* **2** (2016) 31.

[7] K.J. Nichols, A. Van Tosh and C.J. Palestro, *Prospects for advancing nuclear cardiology by means of new detector designs*, *J. Nucl. Cardiol.* **16** (2009) 691.

[8] J.A. Patton, P.J. Slomka, G. Germano and D.S. Berman, *Recent technological advances in nuclear cardiology*, *J. Nucl. Cardiol.* **14** (2007) 13.

[9] E.V. Garcia, T.L. Faber and F.P. Esteves, *Cardiac dedicated ultrafast SPECT cameras: new designs and clinical implications*, *J. Nucl. Med.* **52** (2011) 210.

[10] C.B. Hruska, A.L. Weinmann and M.K. O'Connor, *Proof of concept for low-dose molecular breast imaging with a dual-head CZT gamma camera. Part I. Evaluation in phantoms*, *Med. Phys.* **39** (2012) 3466.

[11] J.A. Kennedy, O. Israel and A. Frenkel, *3D iteratively reconstructed spatial resolution map and sensitivity characterization of a dedicated cardiac SPECT camera*, *J. Nucl. Cardiol.* **21** (2014) 443.

[12] B.A. Herzog et al., *Nuclear myocardial perfusion imaging with a cadmium-zinc-telluride detector technique: optimized protocol for scan time reduction*, *J. Nucl. Med.* **51** (2010) 46.

[13] W.L. Duvall et al., *Reduced isotope dose and imaging time with a high-efficiency CZT SPECT camera*, *J. Nucl. Cardiol.* **18** (2011) 847.

[14] R. Nakazato et al., *Myocardial perfusion imaging with a solid-state camera: simulation of a very low dose imaging protocol*, *J. Nucl. Med.* **54** (2013) 373.

[15] S.S. Gambhir et al., *A novel high-sensitivity rapid-acquisition single-photon cardiac imaging camera*, *J. Nucl. Med.* **50** (2009) 635.

[16] M.F. Smith, *Recent advances in cardiac SPECT instrumentation and system design*, *Curr. Cardiol. Rep.* **15** (2013) 387.

[17] B.F. Hutton, *New SPECT technology: potential and challenges*, *Eur. J. Nucl. Med. Mol. Imag.* **37** (2010) 4.

[18] Z. Keidar et al., *Novel cadmium zinc telluride based detector general purpose gamma camera: initial evaluation and comparison with a standard camera*, *J. Nucl. Med.* **57** (2016) 259.

[19] E. Goshen et al., *Feasibility study of a novel general purpose CZT-based digital SPECT camera: initial clinical results*, *EJNMMI Phys.* **5** (2018) 12.

2019 JINST 14 P02026

[20] M. Sandstrom, I. Ezgi, S. Anders and L. Mark, *Image quality measurements with 177Lu on a GE Discovery 670 CZT*, *J. Nucl. Med.* **58** (2017) 763.

[21] L. Imbert et al., *Compared performance of high-sensitivity cameras dedicated to myocardial perfusion SPECT: a comprehensive analysis of phantom and human images*, *J. Nucl. Med.* **53** (2012) 1897.

[22] S.P. Muller, J.F. Polak, M.F. Kijewski and B.L. Holman, *Collimator selection for SPECT brain imaging: the advantage of high resolution*, *J. Nucl. Med.* **27** (1986) 1729.

[23] F. Weng, S. Bagchi, Q. Huang and Y. Seo, *Design Studies of a CZT-based detector combined with a pixel-geometry-matching collimator for SPECT imaging*, *IEEE Nucl. Sci. Symp. Conf. Rec. (1997)* (2013) 1.

[24] A. Suzuki et al., *A four-pixel matched collimator for high-sensitivity SPECT imaging*, *Phys. Med. Biol.* **58** (2013) 2199.

[25] Y.J Lee and H.J Kim, *Comparison of a newly-designed stack-up collimator with conventional parallel-hole collimators in pre-clinical CZT gamma camera systems: a Monte Carlo simulation study*, *J. Korean Phys. Soc.* **65** (2014) 1149.

[26] C. Robert et al., *Simulation-based evaluation and optimization of a new CdZnTe gamma-camera architecture (HiSens)*, *Phys. Med. Biol.* **55** (2010) 2709.

[27] K. Ogawa and M. Muraishi, *Feasibility study on an ultra-high-resolution SPECT with CdTe detectors*, *IEEE Trans. Nucl. Sci.* **57** (2010) 17.

[28] G. Zeng and D. Gagnon, *Image reconstruction algorithm for a spinning strip CZT SPECT camera with a parallel slat collimator and small pixels*, *Med. Phys.* **31** (2004) 13.

[29] I. Kuvvetli and C. Budtz-Jørgensen, *Measurements of charge sharing effects in pixilated CZT/CdTe detectors*, *IEEE Nucl. Sci. Symp. Conf. Rec.* **N47** (2007) 2252.

[30] M.C. Veale et al., *Measurements of charge sharing in small pixel CdTe detectors*, *Nucl. Instrum. Meth.* **A 767** (2014) 218.

[31] K. Erlandsson, K. Kacperski, D.V. Gramberg and B.F. Hutton, *Performance evaluation of D-SPECT: a novel SPECT system for nuclear cardiology*, *Phys Med Biol,* **54** (2009) 2635.

[32] M.A. Park et al., *Performance of a high-sensitivity dedicated cardiac SPECT scanner for striatal uptake quantification in the brain based on analysis of projection data*, *Med. Phys.* **40** (2013) 042504.

[33] S. Ja et al., *GATE: a simulation toolkit for PET and SPECT*, *Phys. Med. Biol.* **49** (2004) 4543.

[34] K. Thielemans, *STIR: Software for Tomographic Image Reconstruction Release 2*, *IEEE Nucl. Sci. Symp. Conf. Rec.* **M06** (2006) 2174.

[35] B.M. Fuster et al., *Integration of advanced 3D SPECT modeling into the open-source STIR framework*, *Med. Phys.* **40** (2013) 092502.

[36] B.F. Hutton and Y.H. Lau, *Application of distance-dependent resolution compensation and post-reconstruction filtering for myocardial SPECT*, *Phys. Med. Biol.* **43** (1998) 1679.

[37] E.C. Frey, *Collimator detector response compensation in SPECT*, in *Quantitative Analysis in Nuclear Medicine Imaging*, H. Zaidi ed., Springer, Germany (2006).

[38] S. Ben-Haim et al., *Simultaneous dual-radionuclide myocardial perfusion imaging with a solid-state dedicated cardiac camera*, *Eur. J. Nucl. Med. Mol. Imag.* **37** (2010) 1710.

[39] C.B. Hruska and M.K. O'Connor, *A Monte Carlo model for energy spectra analysis in dedicated nuclear breast imaging*, *IEEE Trans. Nucl. Sci.* **55** (2008) 491.

2019 JINST 14 P02026

[40] S.G. Fritz and P.M. Shikhaliev, *CZT detectors used in different irradiation geometries: simulations and experimental results*, *Med. Phys.* **36** (2009) 1098.

[41] X. Zheng, Z. Cheng, M. JamalDeen and H. Peng, *Improving the spatial resolution in CZT detectors using charge sharing effect and transient signal analysis: simulation study*, *Nucl. Instrum. Meth.* **A 808** (2016) 60.

[42] K. Iniewski et al., *Modeling charge-sharing effects in pixellated CZT detectors*, *IEEE Nucl. Sci. Symp. Conf. Rec.* (2007) 4608.

[43] A.E. Bolotnikov et al., *Charge loss between contacts of CdZnTe pixel detectors*, *Nucl. Instrum. Meth.* **A 432** (1999) 326.

[44] B. Zhang and G.L. Zeng, *High-resolution versus high-sensitivity SPECT imaging with geometric blurring compensation for various parallel-hole collimation geometries*, *IEEE Trans. Inf. Technol. Biomed.* **14** (2010) 1121.

[45] Y.H. Lau, B.F. Hutton and F.J. Beekman, *Choice of collimator for cardiac SPET when resolution compensation is included in iterative reconstruction*, *Eur. J. Nucl. Med.* **28** (2000) 39.

[46] F. Weng et al., *An energy-optimized collimator design for a CZT-based SPECT camera*, *Nucl. Instrum. Meth.* **A 806** (2016) 330.

[47] A. Makeev et al., *Evaluation of position-estimation methods applied to CZT-based photon-counting detectors for dedicated breast CT*, *J. Med. Imag.* **2** (2015) 1.

[48] M.E. Myronakis and D.G. Darambara, *Monte Carlo investigation of charge-transport effects on energy resolution and detection efficiency of pixelated CZT detectors for SPECT/PET applications*, *Med. Phys.* **38** (2011) 455.

[49] Philips Healthcare, *Philips BrightView X and XCT specifications*, Netherlands: Koninklijke Philips Electronics N.V. (2009).

[50] GE.Healthcare, *GE Infinia brochure data sheet*, Release 2.5, Direction 2411980-100 Rev3 (2006).

2019 JINST 14 P02026